Journal of Aerosol Science 105 (2017) 35–47

Contents lists available at ScienceDirect

Journal of Aerosol Science

journal homepage: www.elsevier.com/locate/jaerosci

Modeling studies on coagulation of charged particles and comparison with experiments

K. Ghosh[a], S.N. Tripathi[a,b,*], Manish Joshi[c], Y.S. Mayya[d], Arshad Khan[c], B.K. Sapra[c]

[a] Department of Civil Engineering, IIT, Kanpur 208 016, India
[b] Centre for Environmental Science and Engineering, IIT, Kanpur 208 016, India
[c] Radiological Physics and Advisory Division, Bhabha Atomic Research Centre, Mumbai 400 085, India
[d] Department of Chemical Engineering, IIT Bombay, Mumbai 400 076, India

ARTICLE INFO

Keywords:
Charged particles
Coagulation
Nebulization
Particle charge distribution
Boltzmann distribution function

ABSTRACT

A generalized formulation for coagulation of charged particles is presented in this paper. The governing equations can be solved semi-implicitly for a number of discrete size and charge bins. The computationally efficient mechanism gives volume and charge conserved solution with time. A distinct way of handling electrostatic dispersion in dynamic model has been used in this work. The scheme has been tested for charged, nebulized aerosol particles by model studies and also compared with experimental observations. The model simulated results show that charge can significantly affect the coagulation dynamics if charge level is higher than the Boltzmann equilibrium charge limit for less than 1 μm particles. It was found that for the bipolar charge case, there was a significant effect on the enhancement of the coagulation process. For the case of unipolar charge, electrostatic dispersion was seen to play a role in the depletion of number concentration. The model was then validated against results of six controlled experiments in which electrical low pressure impactor (ELPI) was used for measurement of charge and number size distribution. Our model results were found to be in reasonable agreement with observed values. The developed model is fast (independent of time step) and numerically stable. It can be used for several applications involving coagulation dynamics of charged aerosol particles.

1. Introduction

Aerosol particles acquire charge due to various mechanisms (natural and man-made). In the atmosphere, galactic cosmic rays lead to the generation of charged aerosol particles (Laakso, Makela, Pirjola & Kulmala, 2002). Ambient aerosol particles are generally bipolar charged due to the random interaction between positive and negative ions with aerosols (Dhanorkar & Kamra, 2001). Charge on aerosol particles plays an important role in global atmospheric electrical circuit and cloud microphysics (Tinsley, 2008). Industrial processes such as atomization of solutions, mechanical dispersion of powders and metal burning etc. deal with significant amount of charge on aerosol particles (Kousaka, Okuyama, Adachi & Ebie, 1981; Tsai & Lin 2005). For instance, (Hinds & Kennedy, 2000) reported as high as 240,000 excess positive charge/particle generated on aluminium oxide optical powders. The role of charge in determining the dynamical behaviour of aerosol particles can't be ruled out. For example, reduction of agglomeration during the nanoparticle generation in electro-spray technique was achieved by using the highly charged drop as substrate (Ahn et al., 2001; Nakaso et al., 2003). Similarly better understanding of electro coagulation technique via bipolar charging could be utilized for enhancing aerosol collection (Borra et al., 1999). Increasing use of ionizers in air cleaning technologies (Joshi & Sapra 2010;

* Corresponding author at: Department of Civil Engineering, IIT, Kanpur 208 016, India.
E-mail address: snt@iitk.ac.in (S.N. Tripathi).

http://dx.doi.org/10.1016/j.jaerosci.2016.11.019
Received 25 March 2016; Received in revised form 26 September 2016; Accepted 29 November 2016
Available online 06 December 2016
0021-8502/

Nomenclature

(i,j)	size classes of model input particles
(l,m)	charge categories for model input particles
A	Hamaker constant
$A_{chamber}$	area of the chamber
$A_{top,side,floor}$	surface area
C	concentration of particle
C_c	Cunningham correction factor
D	diffusion coefficient of particles
d_a	diameter of air
d_f	fan diameter
d_p	diameter of particle
d_s	stopping distance
e	elementary charge (Coulombs)
f	particle volume fraction
K	Boltzmann constant
k	size classes of new particles
N	fan speed
N_C	number of charge bin
N_S	number of size bin
Q	new charge categories after charge coagulation
$R_{i,j}$	summation between two colliding particle radius
R_i	radius of particles size class i
R_j	radius of particles size class j
r_m	distance between the centers of the colliding particles
T	temperature
t	coagulation time
U	volume of particle
u^*	frictional velocity
$V_{chamber}$	chamber volume
v_E	velocity due to electrical effect
v_g	gravitational settling velocity
ν_{ki}	kinematic viscosity
$v_{top,side,floor}$	deposition velocities on surfaces
z	elementary charge on particles
Z_p	electrical mobility of charged particles

Greek letters

α	correction factor due to charge
β	coagulation coefficient
$\delta_{l,m}$, $\delta_{l+m,Q}$	Kronecker delta function with respect to charges
ϵ_0	permitivity of free space
ϵ_r	dielectric constant of species
ϵ_t	turbulent energy dissipation rate
η	dynamic viscosity
λ	particle deposition rate
$\phi(r_m)$	collision potential due to charge on particles
ρ_p	density of particles

Grinshpun, Adhikari, Honda, Kim, Toivola, Rao & Reponen, 2007) and potent applications for advanced aerosol generation techniques e.g. Electro Hydro Dynamic Atomization (EHDA) (Erven et al., 2005) and glowing wire induced nano-aerosol generation (Khan et al., 2014) also calls for study of charged particles and the possible effect on coagulation dynamics. In another direction, extension of models (Mayya & Sapra, 2004) involving charged particle coagulation could be a crucial step towards better understanding of the governing processes.

Coagulation process is one of the important phenomena of aerosol particle growth. Charge on aerosol particles can affect particle coagulation significantly. For unipolar charged aerosol particles, the coagulation process is suppressed by electrostatic repulsion force. Whereas for bipolar charged particles, coagulation process is enhanced due to several electrical forces like Coulomb attraction force, ion-induced Van der Waal's force and image force. Several experimental studies have investigated the effect of charge on characteristics and dynamics of aerosol particles (Ellasson, Egli, Ferguson & Jodeit 1987; Dhanorkar & Kamra, 2001; Simones et al., 2014; Simones and Loyalka, 2015). Development of coagulation dynamic equation incorporating charge effects started with the work of (Zebel, 1958), who first combined diffusion and coulomb attractions. Fuchs further extended theoretical developments by including free molecular effects (Fuks, 1989). Adachi et al. (1981) developed a two dimensional sectional model for coagulation of charged, mono-dispersed aerosol particles using charge kernels for Coulomb attraction force and image force demonstrating higher depletion rates for the case of bipolar charged particles. Xiong et al. (1992) and Fujimoto et al. (2003) showed that the unipolar charge can reduce the particle growth and also narrow the particle size distribution when electrical dispersion is neglected. Laakso et al. (2002) developed a module for coagulation of charged particles, which is considered as the standard model for atmospheric applications around the world. It is based on the latest charge coagulation kernels (Coulomb force, Image force and ion-induced Vander Waal's force) for collision between multi-sized and multi-charged aerosol particles. Till date, many theoretical coagulation models have been developed based on methods like moment moment (Friedlander, 1983), spline (Gelbard and Seinfeld, 1978) modal (Whitby & McMurry, 1997), sectional (Gelbard & Seinfeld, 1980), Monte-Carlo (Smith, Lee & Matsoukas, 1999) etc. Among these the most accurate method, which is widely used today, is the sectional method. Apart from these, various numerical schemes have also been adopted for developing faster and more accurate coagulation models (Williams & Loyalka). Methods based on sectional method (Vemury, Janzen & Pratsinis, 1997; Laakso et al., 2002) and moment method (Park, Lee, Shimada & Okuyama 2005) mostly were computationally intensive. At present, widely accepted model for coagulation process is the one described by Jacobson, Turco, Jensen and Toon (1994) providing a non-iterative and volume conserved solution.

Models developed for solving charged particle coagulation equation are generally based on several assumptions with respect to size of initial particles, charge level, coagulation kernel etc. Incorporation of size dependent background deposition and electrostatic dispersion in coagulation dynamics, becomes crucial when charge effects supplement the deposition dynamics. For such cases, coagulation and wall loss together forms a formidable part of aerosol dynamic equation (McMurry & Rader, 1985; Shimada et al., 1989; Alonso & Alguacil, 2007). A way of combining electrical repulsion was earlier proposed by Mayya et al. (2004) in the context of air cleaning applications. However it has never been incorporated as a part of aerosol dynamical equation and has never been numerically examined. Despite the wide availability of computational data and models, there are very few studies which focuses on

generating precise experimental data and validating models for charged particle coagulation. This is due to the limitation of measuring charge levels and their microscopic changes during experiments. Some indirect methods like electrostatic deposition have been used by Jiang, Lee and Biswas (2007) and Fujimoto et al. (2003). However, in recent times, the nanometer aerosol differential mobility analyzer (Nano-DMA) (Chen et al., 1998; Lee et al., 2005) and electrical low pressure impactor (ELPI) (Keskinen, Pietarinen & Lehtimaki, 1992) have been used for charge measurements. But in a scenario such as coagulation, the charge distribution changes too fast and performing on-line mobility analysis becomes virtually impossible. On the other hand, although ELPI measures the average charge on individual stages, its capability to measure the charge and number size distributions at high frequencies can be utilized for above mentioned scenarios. Aerosol generated from atomization can be used to understand the impact of charge on the dynamical behavior particularly for chamber applications (Adachi, Okuyama & Kousaka, 1981; Tsai, Lin, Deshpande & Liu, 2005). It is always interesting and useful to study the significance of incorporating (or ignoring) charge in coagulation processes for aerosol growth and dynamics models.

In the present study, we have developed a discrete sectional coagulation model for charged particles where every size category is divided into several charge categories. Computational modification was made so as to formulate a dynamic semi implicit scheme providing volume and charge conserved solution in optimal time. For background deposition, we used (Crump & Seinfeld, 1981) model and fan model (Shimada et al., 1989). Which is similar as described in Sapra et al. (2008). Electrostatic dispersion (important for unipolar charged particles) has been added as an additional deposition velocity term modifying these approaches. The model includes the latest coagulation kernels and it is well adjustable, for investigation of charge particle coagulation process in the atmosphere as well as in chamber experiments. Coagulation of unipolar and bipolar charge particles with Boltzmann/bipolar charge distribution was studied as a test run for the model. For validation, we carried out experiments with atomized NaCl aerosol in controlled closed chamber condition. Measurements made using ELPI in terms of number concentration and number (and charge) size distribution were used for comparisons with theoretical predictions. Measured parameter (including charge) during the experiment assisted in initial parameterization and the background deposition calculation for the model. The model developed under this work can be used as a standalone as well as coupled module for applications oriented towards aerosol growth and dynamics.

2. Model description

2.1. Equation for coagulation of charged particles

The dynamic equation describing behavior of charged aerosol particles under the action of coagulation and other loss terms (including electrostatic dispersion) can be expressed as (1) (Oron & Seinfeld, 1989; Fujimoto et al., 2003).

$$\frac{\partial C(p,U,t)}{\partial t} = \frac{1}{2}\sum_{q=-\infty}^{\infty}\int_0^U \beta_{U-\overline{U},\overline{U}}^{p-q,q} C(p-q,U-\overline{U},t)C(q,\overline{U})d\overline{U} - C(p,U)\sum_{q=-\infty}^{\infty}\int_0^{\infty}\beta_{U,\overline{U}}^{p,q}C(q,\overline{U})d\overline{U} - \lambda(p,U,t)C(p,U,t) \tag{1}$$

Left-hand side of this equation is the rate of change of number concentration of particles of volume U having p elementary charges. The first two terms on the right-hand side of (1) corresponds to the formation and loss of particle of volume U and charge p due to coagulation. The last term accounts for the depositional losses due to diffusion, gravitational settling and electrostatic dispersion (Crump & Seinfeld, 1981; Fuchs, 1964) and (Adachi et al., 1981). This term was formulated by using fan model similar to the approach used in Sapra et al. (2008). For a rectangular closed chamber of volume $V_{chamber}$, loss rate can be calculated using the deposition velocities towards different surfaces as shown below.

$$\lambda(p,U,t) = [A_{top}v_{top}(p,U,t) + A_{floor}v_{floor}(p,U,t) + A_{side}v_{side}(p,U,t)]/V_{chamber} \tag{2}$$

where λ is the particle deposition rate; A_{top}, A_{floor} and A_{side} are the surface areas of the top, floor and walls of the rectangular chamber; v_{top}, v_{floor} and v_{side} are the deposition velocities of particles calculated at respective portions of the chamber. Corresponding v_{side}, v_{top} and v_{floor} are given by

$$v_{side}(p,U,t) = \frac{u^* + v_E}{1 + \frac{u^*}{v_E}\left[1 - exp\left\{-\delta\frac{v_E}{D}cot^{-1}\left(\frac{d_s}{\delta}\right)\right\}\right]} \tag{3}$$

$$v_{top}(p,U,t) = \frac{u^* - v_g + v_E}{1 + \frac{u^*}{v_E - v_g}\left[1 - exp\left\{-\delta\frac{v_E - v_g}{D}cot^{-1}\left(\frac{d_s}{\delta}\right)\right\}\right]} \tag{4}$$

$$v_{floor}(p,U,t) = \frac{u^* + v_g + v_E}{1 + \frac{u^*}{v_E + v_g}\left[1 - exp\left\{-\delta\frac{v_E + v_g}{D}cot^{-1}\left(\frac{d_s}{\delta}\right)\right\}\right]} \tag{5}$$

where v_E is the electrical drift velocity (accounting for enhanced deposition as an effect of charge on aerosol particle), described as

$$v_E = \frac{V_{chamber}}{A_{chamber}\epsilon_0} Z_p(p, U) \sum_{q=-\infty}^{\infty} \int_0^{\infty} qC(q, \overline{U}, t) d\overline{U} \tag{6}$$

Z_p in the above equation is the electrical mobility of charged particles, $A_{chamber}$ is the area of chamber and ϵ_0 is the permitivity of free space. As mentioned above, deposition velocities shown in Eqs. (3), (4), and (5) combines electrostatic dispersion with other deposition processes. δ used in the above equations is given by

$$\delta = (D/k_e)^{1/2} \tag{7}$$

where D is the diffusion coefficient of particles and k_e is given by

$$k_e = 0.4\left(2\frac{\epsilon_t}{15\nu_{ki}}\right)^{1/2} \tag{8}$$

k_e depends on ν_{ki} (kinematic viscosity) and ϵ_t (turbulent energy dissipation rate) which is given by

$$\epsilon_t = \frac{N^3 d_f^5}{V_{chamber}} \tag{9}$$

where N and d_f are the rotational speed and diameter of the fan inside the chamber respectively. In Eqs. (4) and (5), ν_g is the gravitational settling velocity, and is given by

$$v_g = \frac{2}{9}\frac{(\rho_p - \rho_a) g r^2 C_c}{\eta} \tag{10}$$

With ρ_p and ρ_a denoting the density of particle and air respectively, and η is the dynamic viscosity. In Eq. (4) and (5) d_s, the stopping distance of particle, is given by

$$d_s = \frac{u^* \rho_p d_p^2 C_c}{18\eta} \tag{11}$$

where d_p is the particle diameter, C_c is the Cunningham correction factor and u^* is the friction velocity denoting the effect of turbulent deposition in terms of fan parameters and is given by

$$u^* = (N d_f^2)/V_{chamber}^{1/3} \tag{12}$$

Being an integro-differential non-linear Eq. (1), analytical solution exists for assumptive cases only (Anand & Mayya, 2009). However, several numerical schemes like sectional method (Gelbard & Seinfeld, 1980), nodal method (Jacobson et al., 1994) etc, have been developed for solving this equation in the past. Coagulation kernel can be modified by incorporating charge effect terms and the modified kernel can then be used in numerical scheme.

In this work, coagulation model was formulated by adding charge term into equation reported by Jacobson et al. (1994) giving volume and charge conserved, semi implicit formula, described as

$$U_k C_k^Q(t+1) = \frac{U_k C_k^Q(t) + \Delta t \sum_{l,m=Q_{min}}^{l,m=Q_{max}} \left[\sum_{j=1}^{k} \left\{ \sum_{i=1}^{k-1} \frac{f_{i,j,k}\delta_{l+m,Q}}{1+\delta_{l,m}} \beta_{i,j}^{l,m} U_i C_i^l(t+1) C_j^m(t) \right\} \right]}{1 + \Delta t \left[\sum_{m=1}^{N_C} \left\{ \sum_{j=1}^{N_S} (1 - f_{k,j,k}) \beta_{k,j}^{l,m} C_j^m(t) \right\} + \lambda_k^Q(t) \right]} \tag{13}$$

The above model (equation no. (13)) was well validated with severel publishe models (Laakso et al., 2002; Palsmeier & Loyalka, 2013). The second numerator and denominator term in RHS. are the production and loss term due to charge particle coagulation respectively, the last denominator term in RHS is the loss term due to combine deposition process. Where i and j are size classes of two model input particles and k is the size class of new particles formed after coagulation. C is the time dependent number concentration,UC is the volume concentration of particles, U is the volume of particle, N_S is the number of logarithm bins for size of particle, Δt is the time-step, superscript t and t+1 represents initial and final concentrations respectively, $\beta_{i,j}^{l,m}$ is charge coagulation coefficient, N_C is the number of bins for charge categories, Q is the new charge category arising due to coagulation between two model charge categories l and m. $\delta_{l,m}$ and $\delta_{l+m,Q}$ are the Kronecker delta function with respect to charges, given by

$$\delta_{l+m,Q} = \begin{cases} 0, & l+m \neq Q \\ 1, & l+m = Q \end{cases} \tag{14}$$

$$\delta_{l,m} = \begin{cases} 0, & l \neq m \\ 1, & l = m \end{cases} \tag{15}$$

The volume fraction, $f_{i,j,k}$, is given by

$$f_{i,j,k} = \begin{cases} \left(\frac{U_{k+1}-U_{i,j}}{U_{k+1}-U_k}\right)\frac{U_k}{U_{i,j}} & U_k \le U_{i,j} < U_{k+1} (k < N_S) \\ 1 - f_{i,j,k-1} & U_{k-1} < U_{i,j} < U_k (k > 1) \\ 1 & U_{i,j} \ge U_k (k = N_S) \\ 0 & \text{all other cases} \end{cases} \tag{16}$$

In Eq. (16), the fraction works with all types of input size distributions like monomer, geometric and random. Here $U_{i,j}$ is given by

$$U_{i,j} = U_i + U_j \tag{17}$$

2.2. Kernel for charged particle coagulation

To calculate the kernel for coagulation of charged particles, first we calculated the correction factor due to charge based on all electrical forces, from (Laakso et al., 2002) and (Mick et al., 1991) than updated it into the Brownian coagulation kernel. The updated Kernel for charged particle coagulation is given by

$$\beta_{i,j}^{l,m} = \alpha_{i,j}^{l,m} \beta_{i,j}^{B} \tag{18}$$

Where $\alpha_{i,j}^{l,m}$ is the correction due to charge and $\beta_{i,j}^{B}$ is the particle Brownian coagulation coefficient. $\beta_{i,j}^{B}$ includes all transition corrections as proposed by Fuchs using interpolation formula.

2.2.1. Correction factor due to charge

The correction factor $\alpha_{i,j}^{l,m}$ was calculated from electrostatic, image and ion induced Van der Waal's forces due to charge on particle in accordance with reported literature (Howard et al., 1973; Ball and Howard, 1971; Mick et al., 1991) and (Laakso et al., 2002). In the case of repulsive force, correction factor was taken from Laakso et al. (2002). After dimensional analysis; the correction factor with respect to both size and charge was reformed as:

$$\alpha_{i,j}^{l,m} = exp\left[\frac{-\phi_{i,j}^{l,m}(r_m)}{KT}\right] \tag{19}$$

In all other cases (valid for collision between neutral and charged particles also), the rearranged form will be

$$\alpha_{i,j}^{l,m} = \frac{r_m^2(1 - \phi_{i,j}^{l,m}(r_m)/KT)}{R_{i,j}^2} \tag{20}$$

where $R_{i,j}$ is summation of R_i (radius of the particles for i size class) and R_j (radius of the particles for j size class). For repulsive case, in Eq. (19) r_m is the value where collision potential ϕ becomes maximum. In Eq. (20), r_m is the value where right hand side numerator reaches its minimum value. The collision potential $\phi(r)$ is

$$\phi(r_m) = \phi_{es}(r_m) + \phi_{img}(r_m) + \phi_{vdw}(r_m) \tag{21}$$

where $\phi_{es}(r_m)$ is the collision potential for electrostatic force, $\phi_{img}(r_m)$ is the collision potential for electrical image force and $\phi_{vdw}(r_m)$ is the ion induced Van der Waals force described by Mick et al. (1991), and further modified by Laakso et al. (2002) for multi sized particles. The Van der Waal's collision potential is given by

$$\phi_{vdw}(r_m) = \frac{-A}{6}\left[\frac{2R_iR_j}{r_m^2 - (R_i + R_j)^2} + \frac{2R_iR_j}{r_m^2 - (R_i - R_j)^2} + ln\left(\frac{r_m^2 - (R_i + R_j)^2}{r_m^2 - (R_i - R_j)^2}\right)\right] \tag{22}$$

where A is the Hamaker constant for NaCl particle (Israelachvili, 1992), r_m is the distance between the center of the two colliding particles. Equation for electrostatic collision potential is given by

$$\phi_{es}(r_m) = \frac{e^2}{4\pi\epsilon_0} z_i z_j \frac{1}{R_{i,j}} \tag{23}$$

where ϵ_0 is permittivity of free space and z_i, z_j are the number of elementary charges for particle size i and j, respectively. The collision potential for electrical image force is described as

$$\phi_{img}(r_m) = \frac{\epsilon_r - 1}{\epsilon_r + 1}\frac{e^2}{8\pi\epsilon_0}\left\{(p_{ii} - 1/R_i)z_i^2 + 2p_{ij}z_iz_j + (p_{jj} - 1/R_j)z_j^2 - \frac{2z_iz_j}{R_{ij}}\right\} \tag{24}$$

where ϵ_r is the dielectric constant of the species. $p_{ii} = q_{jj}/\omega$, $p_{jj} = q_{ii}/\omega$, $p_{ij} = -q_{ij}/\omega$, $\omega = q_{ii}q_{jj} - q_{ij}^2$. q_{ii} and q_{jj} are given by

$$q_{ii} = R_i(1 - \eta_{img}) \sum_{m=0}^{\infty} [\theta^m/(1 - \eta\theta^{2m})] \tag{25}$$

$$q_{jj} = R_j(1 - U_{img}) \sum_{m=0}^{\infty} [\theta^m/(1 - U\theta^{2m})] \tag{26}$$

$$q_{ij} = -(R_iR_j/r - m)(1 - \theta^2) \sum_{m=0}^{\infty} [\theta^m/(1 - \theta^{2m+2})] \tag{27}$$

where $U_{img} = [(R_j + R_i\theta)/r_m]^2$, $\eta_{img} = [(R_i + R_j\theta)/r - m]^2$, $\theta = \gamma - (\gamma^2 - 1)^{1/2}$. γ is given by

$$\gamma = (r^2 - R_i^2 - R_j^2)/2R_iR_j \tag{28}$$

The charge correction factor used in the above formulation provides similar results to that calculated from diffusion-mobiity equation in continuum regime (Fuchs, 1964; Yu & Turco, 1998).

The above numerical scheme (13) is independent of time steps and an accurate for studying temporal changes in size distribution as well as charge distribution, for coagulation and deposition of charged particles in a closed environment. This model is applicable to a wide size distribution (0.01 μm to 1 μm) and large charge level boundaries of ± 20 (in 41 bins). The charge boundary was chosen on the basis of charge limit of ± 20 for a 1 μ atomized particle, according to the ionic fluctuation theory of Smoluchowski (Liu & Pui, 1974). The model was computationally simulated and experimentally validated as a part of this work. Model parameters which were constant during simulations and are shown in Table 1.

3. Experimental setup

Six experiments were carried out in a controlled chamber of 0.5 mtextsuperscript3 volume at ambient conditions. Fig. 1 shows the schematic representation of sampling set-up and instrumentation employed for experiments. Two fans were used to homogenize aerosols inside the chamber. Uniformity of aerosol number concentration was verified taking aerosol samples using CPC from different ports of this chamber. Temperature and Relative Humidity conditions were recorded. NaCl solution (10% w/v) was atomized using TSI atomizer (Model No. 3079) and atomized NaCl aerosols were fed to the chamber through a port using connecting tubes. On the opposite side, ELPI was connected and measurement of number and charge size distributions were made throughout the experiments. ELPI consists of a unipolar charger, impactor and electro-meter assembly. It can measure number and charge size distribution from 6 nm - 10 μm at a frequency of 10 Hz. Charger can be kept off for direct (average) charge size distribution while it must be on for converting measured current changes to number concentration. In our experiments, we timed the charger on-off for alternate 20 seconds so as to measure number size distribution and charge size distribution continuously. Grimm Scanning mobility particle sizer (SMPS) was connected through another port in the chamber. The measurement parameters of SMPS were used for model calculations.

Similar protocol was adopted for all experiments and controlling conditions were maintained nearly same as well. A typical sequence of experiment was to feed atomized aerosols to chamber to achieve number concentration of nearly 10^6 per cm^3 where the atomization was stopped. The initial number size distribution and charge size distribution measured around peak number concentration of each experiment (i.e. at 10^6 per cm^3) by ELPI was used as input conditions for the model v/s experiment comparisions. After atomization was stopped, subsequent measurements were taken in closed chamber condition. For these times, measured parameters were compared with predictions of the model.

4. Results and discussion

4.1. Model calculation results

The charge levels on atomized NaCl aerosols were not modified during the experiments. The model simulations however made at a charge level higher than the experiments for indicative testing (to see the maximum effect of particle charge on coagulation of nebulized particles) but the number concentration was used same as the initial concentration for experiment. Inputs for the model were the particle size distribution obtained from experimental data of the SMPS instrument and charge fraction for different sizes obtained from reported literature ((Liu and Pui, 1974) and (Tsai et al., 2005)). Initial total number concentration of aerosol particle

Table 1
Parameters used for model calculation.

Item	Parameter value
Particle type	Common salt (NaCl)
Density of particle	2.16 gm/cc
Temperature	300 kelvin
Hamaker constant	5.35×10^{-20} joule
Dielectric constant	∽ 63 for 10% NaCl solution (Gavish & Promislow)

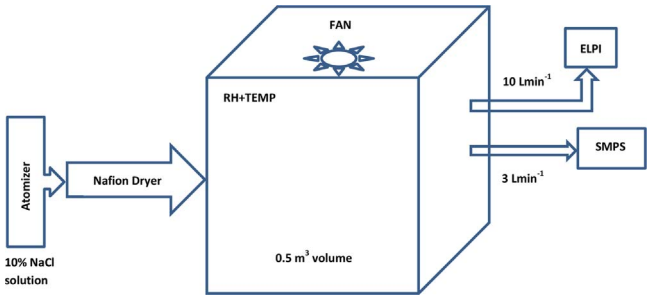

Fig. 1. Experimental setup.

was approximately 10^6 per cm^3 which is good for coagulation studies while initial charge on particles was taken from 1 (for ≦0.1 μm particles) to 20 (for 1 μm particles) which is the maximum mean charge of nebulized water particle at dielectric constant 80 (Liu and Pui, 1974).Then the model for charged particle coagulation (using Eq. (13)) was run for one hour of coagulation time period. The results are shown in Figs. 2 and 3. For charging of aerosol in ionic environment, the charge distribution is given by Boltzmann law for continuum regime (mean free path of ion > size of aerosol) (Gunn, 1955; Keefe et al., 1959); while it takes Gaussian form for free molecular regime (Matsoukas and Russell, 1997). Whereas, mean charge is approximately zero i.e. positive and negative particles for flames and radioactive chargers; charge distribution becomes unipolar for plasmas and interstellar space (Smith et al., 1999). In our work, we studied both possibilities i.e. unipolar and bipolar charged particles as a test case for model. To better understand charge effect, we took three different input charge cases as described below:

4.1.1. Case 1: unipolar charge

For every size, one unipolar (negative or positive) Kronecker delta function was taken (considering charge distribution probability = 1, where model charge bin matches the observed charge level). For this case, effects of electrostatic repulsion in terms of suppression of coagulation rates can be explored.

4.1.2. Case 2: uncharged

Coagulation w/o charge case is simply obtained from Eq. (13) after setting q = 0. Using this, we can determine the extent of charge effect on coagulation process.

4.1.3. Case 3: bipolar charge

It is an enhancement of coagulation case, where for every size, one bipolar Kronecker delta charge distribution (probability = 0.5 for each pole) was taken (Park et al., 2005; Borra et al., 1999).

Fig. 2 compares the coagulation for above discussed cases in terms of depletion of total number concentration with time. Simulation result ignoring electrostatic dispersion has also been plotted for comparison. Uncharged particles (case 2) refer to a scenario where the effect of coagulation increases the size of the particles affecting their background deposition rates, subsequently. This is contrasted with the case of unipolar charged particles (case 1) when electrostatic dispersion is not taken into account. In this case, although diffusional deposition and gravitational settling still operates, the inhibition of coagulation does not allow particle sizes to grow thereby making their depletion rate far slower. When electrostatic dispersion is introduced on unipolar charged case (case 4), highest depletion rates are seen clearly pointing at dominating role of electrostatic dispersion in the removal of particles. It

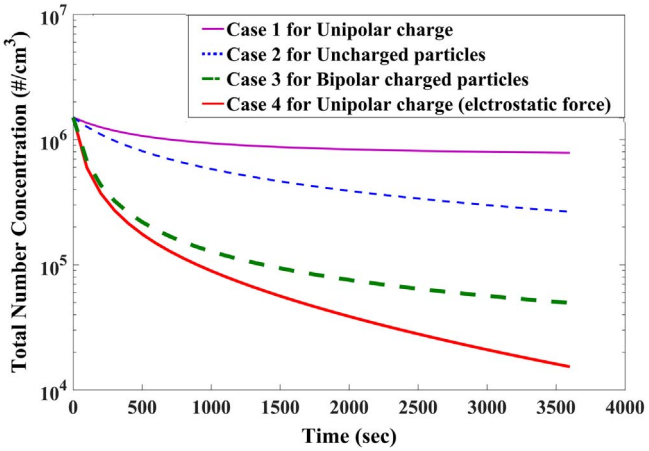

Fig. 2. Model predicted depletion of number concentration inside the chamber.

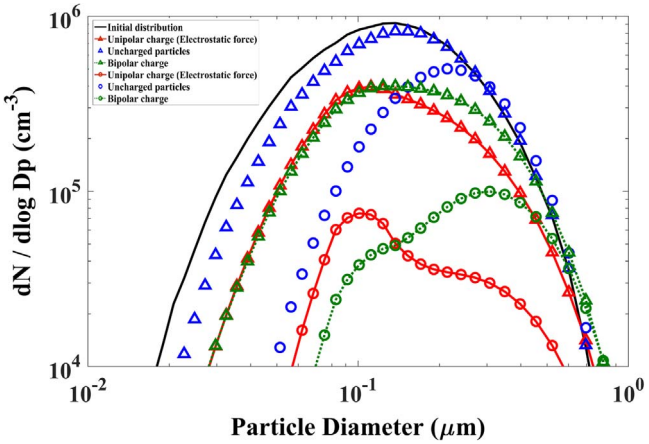

Fig. 3. Model predicted evolved size distribution for 100 sec (Triangular lines) and for 1000 sec (Circular lines).

must be noted that the charge levels introduced are compared favorably with the charges that would be acquired by particles subjected to any unipolar charging such as charging of particles by ionizers (Mayya et al., 2004). For the case of bipolar charged particles (case 3), electrostatic attraction between the unlike charged particles enhances their coagulation rates increasing gravitational precipitation, substantially. It could be inferred that both unipolar and bipolar charging have a potential to increase deposition rate of particles either by introducing electrostatic repulsion or by enhancing coagulation by attraction. These observations confirms the role of electrostatic charge on aerosol dynamics. Also, near parallel slope for uncharged and bipolar charged particles at later times indicate common role of background deposition processes (i. e. loss of charge for bipolar charged particles).

More detailed evidence for above discussed summary conclusions can also be drawn by looking at evolution of size distribution spectra of particles shown in Fig. 3. This figure represents the evolution of particle size distribution after interaction time of 100 and 1000 seconds for above cases (uncharged, unipolar with electrostatic dispersion and bipolar). The change in size distribution was seen to be in accordance with Fig. 2. Highest shift in size distribution was seen for bipolar charged particle case (case 3) followed by the case of uncharged (case 2) and unipolar charged particles (case 1), respectively. For bipolar charge case, charged particle coagulation effect was seen to be pronounced compared to the case of uncharged particles, indicating significant effect of charge on Brownian coagulation of charged aerosols. For this case, evolution of size spectrum can clearly be observed with indication of evolution of secondary mode which got enhanced at 1000 seconds. The effect of unipolar charge (with electrostatic dispersion) on the coagulation (relative to coagulation of bipolar charged particles) could not be seen while comparing size distributions at 100 seconds. However, after allowing coagulation for longer times, modification in size spectrum could be seen, as well mostly in terms of reduction of number concentration. At 1000 seconds, relative effect of charged particle coagulation was clearly seen in narrowing of size distribution for case 1 (i. e. unipolar charged particles) and broadening for case 3 (i. e. bipolar charged particles) as compared to the case of uncharged particles case (case 2). In addition to that, due to the strong effect of electrostatic dispersion, particle deposition enhanced dramatically, as evident in Fig. 2 as well.

Our charged particle coagulation model results show very rapid coagulation effect for bipolar charged particles, similar to results found in reported literature (Palsmeier & Loyalka, 2013). Within 100 sec, the peak number concentration depletes to approximately

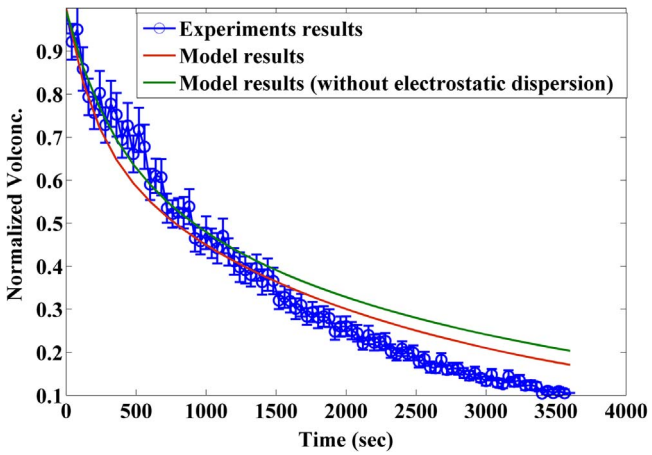

Fig. 4. Effect of deposition on volume concentration for chamber conditions.

three times the initial peak value. On the basis of model results, it can be inferred that for any realistic highly charged nebulized particle system, bipolar charged particle coagulation can significantly change the total number concentration as well as the particle size distribution. On the other-hand, electrostatic dispersion fully dominated in the case of unipolar charged. Subsequently, we tested our model using measurements from experiments carried out with atomized and dried NaCl aerosols as described below.

4.2. Comparison of model and experiment results

The changes in number concentration and particle size distribution for nebulized charged particle were calculated using our charged particle coagulation model (Eq. (13)), and the results were validated against experiments. The standard input conditions used in the model are given in the experimental section.The input particle size distributions were taken from ELPI instruments.We took eleven logarithm size bins (N_S) between 0.01 μm to 1 μm and twenty one linear charge bins (N_C) between −10 to +10. Besides this, we also calculated coagulation for uncharged particle case (case 2) using (Eq. (13)) after setting q = 0. For our experiments, deposition and coagulation both play a significant role in reducing total particle number concentration with time. As coagulation conserves mass, depletion of volume concentration (mass) with time can happen only due to depositions inside the chamber (assuming no change in particle density during this period) (Jacobson et al., 1994). We compared our deposition model results (equation no. (2)) with experimental data, the results for which are shown in Fig. 4.

As observed in Fig. 4, model results for both cases (with or without electrostatic dispersion) were close to the experimental observations. The over-prediction of model at later phase may be due to the fact that the assumption of uniform mixing may not be valid at late times possibly due to the onset of gravitational stratification effects.

Fig. 5 shows the changes in absolute average charge of particle as a function of size of nebulized particle. This figure compares the results obtained from Boltzmann equilibrium charge model calculation (Hinds, 2012) with that of experimental measurements at the peak of total concentration of particles. In our experiments, average absolute charge measured by ELPI instrument closely matched the Boltzmann model calculation results for lower sizes. High concentration of NaCl solution (∽10%) for generating charged aerosol particle could be the reason for the charge level being reasonably close to Boltzmann equilibrium charge (Tsai et al., 2005). However after 0.3 μm, observed charge levels become higher than Boltzmann charge level for all six experiments. So for charged particle coagulation model calculation, we divided the input charge distribution into two cases. For first case, we directly input charge distribution as Boltzmann charge distribution for every size of particle. For second case, we used bipolar delta charge function for every size of particle by taking charge probability distribution = 0.5 (Park et al., 2005; Borra et al., 1999) for each pole, where input model charge levels match with experiment values.

Fig. 6 shows the comparison between the experiment and charged particle coagulation model derived results for depletion in total number concentration of particle with time. For comparison, we have also plotted the results of coagulation model for uncharged particles. Interestingly, we observed that all model results show appreciable agreement with experiment results. This was expected for charged particle coagulation models but not for w/o charge model. On further investigation, we realized that in the experiment, our peak number concentration occurred at 0.1 μm (shown in Fig. 7) and average charge level around 0.1 μm sized particles (see Fig. 5) was very low (∽0.1) for observing significant effect on charged particle coagulation process. Also, there was possibility of mixture of unipolar and bipolar charge distribution. In order to dwell further, we compared particle size distributions for observing charged particle coagulation effects closely, the results for which are shown in Fig. 7.

This figure compares evolution of particle size distribution as an effect of coagulation for interaction time of 2, 20 and 40 min. Here, experimental results have been plotted with model simulations for all cases (uncharged, Boltzmann charged, Bipolar charged particles). The best agreement with experiment data was observed for charged particle (delta bipolar) coagulation model. However, the number concentration peak occurring at approximately 0.1 μm size of particle does not match with any of the simulated results. The pattern was, however, seen to be similar for all time levels. In the case of low charge levels (as in real cases), it is always difficult to determine effect of charge on coagulation dynamics in the presence of background deposition. Incorporating size-dependent background deposition model, we tried to carefully observe even minimal effects of charge on coagulation dynamics. On a gross level

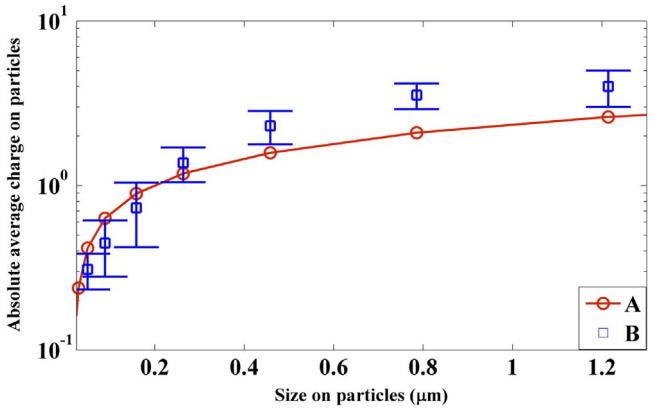

Fig. 5. Effect of particle size on average charge for A) Boltzmann distribution B) Experiments.

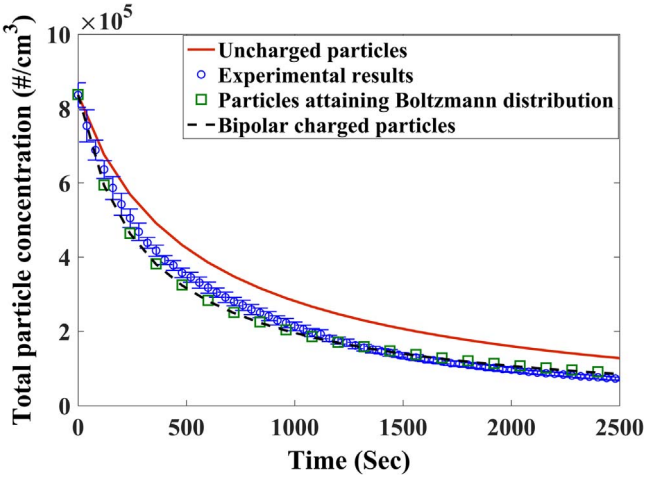

Fig. 6. Depletion of number concentration as an effect of charged particle coagulation: theory and experiment.

(as seen in Figs. 6 and 7), small difference of modifying coagulation kernel was observed, although experimental results were seen to be closer to the charged particle coagulation model. For the next step, to see the charged particle coagulation effect, we chose four particle sizes having relatively higher charge level than Boltzmann equilibrium charge. Results are shown in Fig. 8.

Fig. 8 shows the comparison between model and experiment results for depletion in particle number concentration with time for coagulation of uncharged and charged particles. Four sub-figurers represents four different sizes of aerosol particles: (a) 158 nm, (b) 263 nm, (c) 458 nm and (d) 750 nm (consistent with the mean size of ELPI stages for which charge levels were measured). Out of the three different model calculations, delta bipolar charge model shows closer agreement with experimental values for all four sizes. For 158 nm sized particles, observed charge level was less than Boltzmann charge level, so we found less effect of charge on the coagulation process. For other sizes, it clearly shows that with increasing size of particle, carrying capacity of charge on particle also increases, which leads to an increase in the charged particle coagulation process. In absence of accurate charge distribution data (as we could only measure average charge on particle sizes), the model predictions could not be improved further. Apart from the unexplored deviation of measured charge distribution with respect to assumed charge distribution for higher size particles, another possible reason of observed differences could be gravitational stratification effects. Nevertheless, model results were found to be closer to experimental predictions for all cases. A clear effect of charge was seen on coagulation process in our model calculations which was validated further with our experimental data under limitations for particle sizes less than 1 μm.

5. Conclusion

This work discusses the development of a model which can successfully be used for study the coagulation of charged particles. The developed model has been tested against unipolar and bipolar charge levels on particle sizes. A significant effect of charge on coagulation dynamics was observed while comparing coagulation of uncharged case (case 2) with bipolar case (case 3). In absence of electrostatic dispersion effects, coagulation was seen to be inhibited for unipolar charged particles. However depletion rate was seen to be drastically increasing when electrostatic dispersion was included in the model. Six controlled experiments using nebulized NaCl

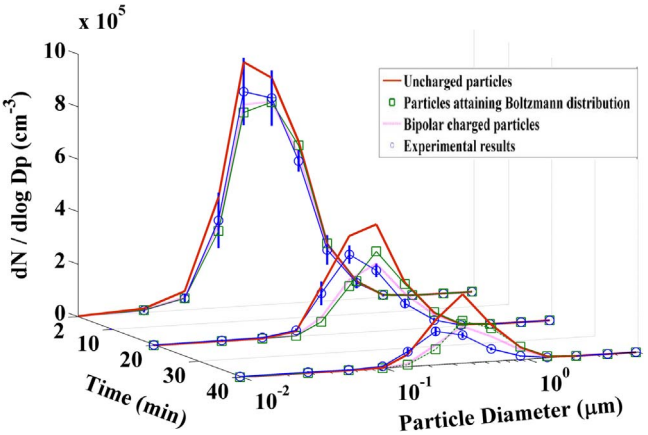

Fig. 7. Evolution of size distribution: theory and experiment.

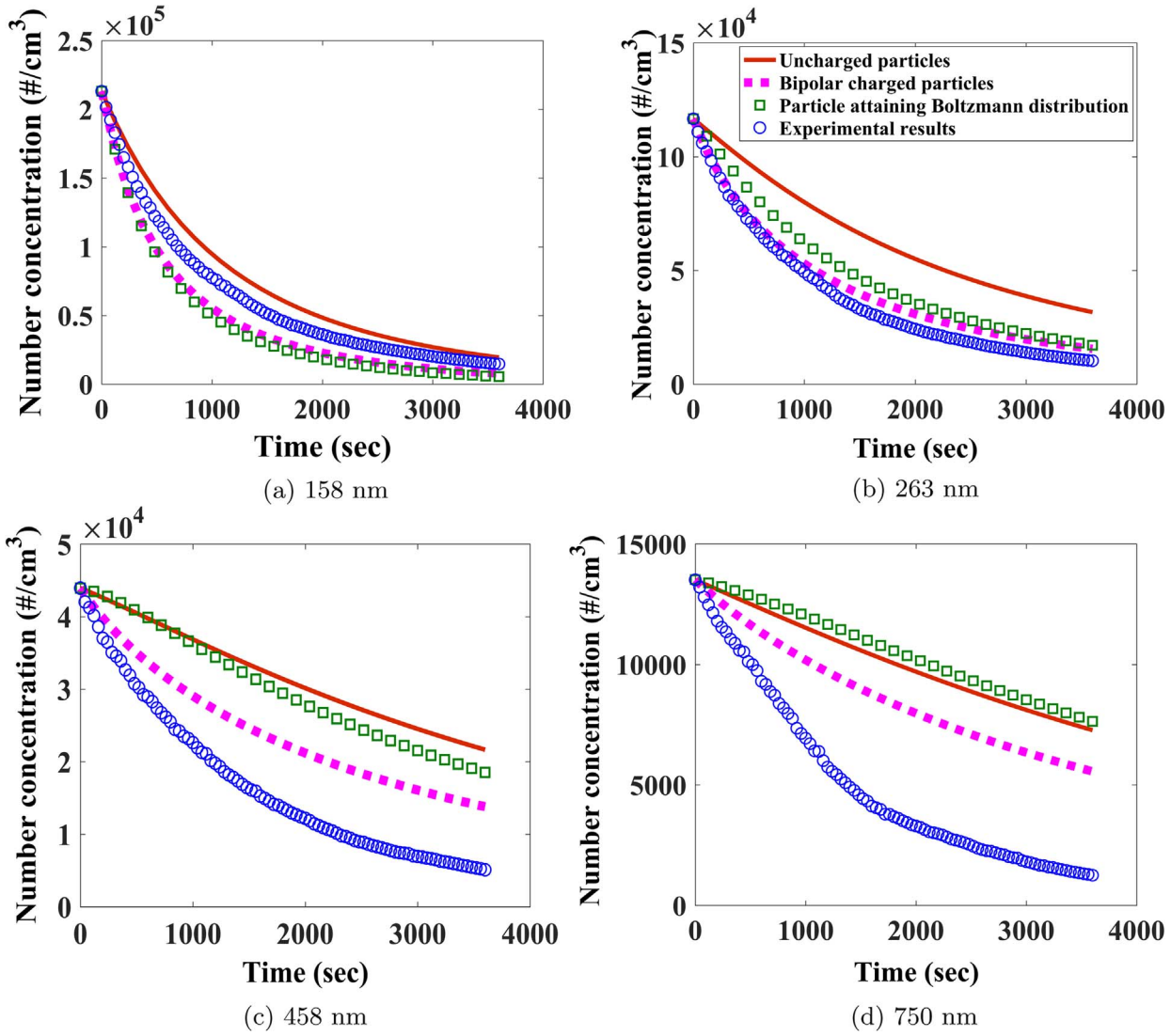

Fig. 8. Depletion of number concentration for different sizes: theory and experiment.

aerosols were performed and the results of the measurements have been used for validating the model. Average charge levels measured on different particle sizes were compared with Boltzmann equilibrium charge distribution and an agreement was seen for lower particle sizes. In absence of measurement of charge size distribution, different cases were assumed for the same. Model was seen to predict charge particle coagulation induced number concentration depletion closely for Boltzmann and bipolar charge cases. However for larger sizes (where the charge carried by particle is relatively higher), delta bipolar charge case was found to be closer to experiments.

The coagulation kernel used in this model includes various depositional effects (settling, diffusion, electrostatic dispersion) in addition to charge correction. In contrast to previous studies, electrostatic dispersion term has been added in the depositional framework itself. Incorporation of size dependent background deposition model provide a realistic frame work for closed chamber dynamics (applications). The results from validation experiments are important in view of role of charge in lung delivery applications. This model can be used as a standard for any charged particle coagulation process application in several domains such as atmospheric applications, surface deposition, particle generation, weather simulation etc.This model based on volume and charge concentration conserved approach provides the user an ability to use of wide range of charge and size distribution for charged particle coagulation with good accuracy.

Acknowledgment

The present study was supported in part by Health, Safety and Environmental group, Bhabha Atomic Research Centre,

Government of India. The authors also gratefully acknowledge the financial support provided by Board of Research in Nuclear Science (BRNS), Department of Atomic Energy (DAE), Government of India to conduct this research under project no. 36(2,4)/15/01/2015-BRNS.

References

Adachi, M., Okuyama, K., & Kousaka, Y. (1981). Electrostatic coagulation of bipolarly charged aerosol particles. *Journal of Chemical Engineering of Japan*, 14(6), 467–473.

Ahn, K., Yoonm, J., Yang, T., & Choi, M. (2001). Nano sio2 particle agglomeration control in a furnace reactor with electro-spray assisted synthesis. In International Symposium on Nanoparticles: Aerosols and Materials, pp. 64–67.

Alonso, M., & Alguacil, F. J. (2007). Penetration of aerosol undergoing combined electrostatic dispersion and diffusion in a cylindrical tube. *Journal of Aerosol Science*, 38(5), 481–493.

Anand, S., & Mayya, Y. (2009). Coagulation in a diffusing gaussian aerosol puff: comparison of analytical approximations with numerical solutions. *Journal of Aerosol Science*, 40(4), 348–361.

Ball, R., & Howard, J. (1971). Electric charge of carbon particles in flames. In *Symposium (International) on Combustion*, *Vol. 13*, Elsevier, 1971, pp. 353–362.

Borra, J., Camelot, D., Chou, K.-L., Kooyman, P., Marijnissen, J., & Scarlett, B. (1999). Bipolar coagulation for powder production: micro-mixing inside droplets. *Journal of Aerosol Science*, 30(7), 945–958.

Chen, D.-R., Pui, D. Y., Hummes, D., Fissan, H., Quant, F., & Sem, G. (1998). Design and evaluation of a nanometer aerosol differential mobility analyzer (nano-dma). *Journal of Aerosol Science*, 29(5), 497–509.

Crump, J. G., & Seinfeld, J. H. (1981). Turbulent deposition and gravitational sedimentation of an aerosol in a vessel of arbitrary shape. *Journal of Aerosol Science*, 12(5), 405–415.

Dhanorkar, S., & Kamra, A. (2001). Effect of coagulation on the particle charge distribution and air conductivity. *Journal of Geophysical Research: Atmospheres (1984–2012)*, 106(D11), 12055–12065.

Ellasson, B., Egli, W., Ferguson, J., & Jodeit, H. (1987). Coagulation of bipolarly charged aerosols in a stack coagulator. *Journal of Aerosol Science*, 18(6), 869–872.

Erven, J.v., Moerman, R., & Marijnissen, J. C. (2005). Platinum nanoparticle production by ehda. *Aerosol Science and Technology*, 39(10), 941–946.

Friedlander, S. (1983). Dynamics of aerosol formation by chemical reaction*. *Annals of the New York Academy of Sciences*, 404(1), 354–364.

Fuchs, N. (1964). *The mechanisms of aerosols*.

Fujimoto, T., Kuga, Y., Pratsinis, S. E., & Okuyama, K. (2003). Unipolar ion charging and coagulation during aerosol formation by chemical reaction. *Powder technology*, 135, 321–335.

Fuks, N. A. (1989). *The mechanics of aerosols*. Dover Publications.

Gavish, N., & Promislow, K. Dependence of the dielectric constant of electrolyte solutions on ionic concentration, arXiv preprint arXiv:1208.5169

Gelbard, F., & Seinfeld, J. H. (1978). Numerical solution of the dynamic equation for particulate systems. *Journal of Computational Physics*, 28(3), 357–375.

Gelbard, F., & Seinfeld, J. H. (1980). Simulation of multicomponent aerosol dynamics. *Journal of Colloid and Interface Science*, 78(2), 485–501.

Grinshpun, S. A., Adhikari, A., Honda, T., Kim, K. Y., Toivola, M., Ramchander Rao, K., & Reponen, T. (2007). Control of aerosol contaminants in indoor air: combining the particle concentration reduction with microbial inactivation. *Environmental Science Technology*, 41(2), 606–612.

Gunn, R. (1955). The statistical electrification of aerosols by ionic diffusion. *Journal of Colloid Science*, 10(1), 107–119.

Hinds, W. C., & Kennedy, N. J. (2000). An ion generator for neutralizing concentrated aerosols. *Aerosol Science Technology*, 32(3), 214–220.

Hinds, W. C. (2012). *Aerosol technology: properties, behavior, and measurement of airborne particles*. John Wiley & Sons.

Howard, J., Wersborg, B., & Williams, G. (1973). Coagulation of carbon particles in premixed flames. *Faraday Symposia of the Chemical Society*, 7, 109–119.

Israelachvili, J. N. (1992). *Intermolecular and surface forces: With applications to colloidal and biological systems (colloid science)*.

Jacobson, M. Z., Turco, R. P., Jensen, E. J., & Toon, O. B. (1994). Modeling coagulation among particles of different composition and size. *Atmospheric Environment*, 28(7), 1327–1338.

Jiang, J., Lee, M.-H., & Biswas, P. (2007). Model for nanoparticle charging by diffusion, direct photoionization, and thermionization mechanisms. *Journal of Electrostatics*, 65(4), 209–220.

Joshi, M., Sapra, B., Khan, A., Kothalkar, P., & Mayya, Y. (2010). Thoron (220 rn) decay products removal in poorly ventilated environments using unipolar ionizers: dosimetric implications. *Science of the Total Environment*, 408(23), 5701–5706.

Keefe, D., Nolan, P.J., & Rich, T.A. (1959). Charge equilibrium in aerosols according to the boltzmann law. In Proceedings of the Royal Irish Academy. Section A: *Mathematical and Physical Sciences, JSTOR*, pp. 27–45.

Keskinen, J., Pietarinen, K., & Lehtimäki, M. (1992). Electrical low pressure impactor. *Journal of Aerosol Science*, 23(4), 353–360.

Khan, A., Modak, P., Joshi, M., Khandare, P., Koli, A., Gupta, A., Anand, S., & Sapra, B. (2014). Generation of high-concentration nanoparticles using glowing wire technique. *Journal of Nanoparticle Research*, 16(12), 1–8.

Kousaka, Y., Okuyama, K., Adachi, M., & Ebie, K. (1981). Measurement of electric charge of aerosol particles generated by various methods. *Journal of Chemical Engineering of Japan*, 14(1), 54–58.

Laakso, L., Mäkelä, J. M., Pirjola, L., & Kulmala, M. (2002). Model studies on ion-induced nucleation in the atmosphere. *Journal of Geophysical Research: Atmospheres (1984–2012)*, 107(D20) (AAC-5).

Lee, H. M., Kim, C. S., Shimada, M., & Okuyama, K. (2005). Bipolar diffusion charging for aerosol nanoparticle measurement using a soft x-ray charger. *Journal of Aerosol Science*, 36(7), 813–829.

Liu, B. Y., & Pui, D. Y. (1974). Electrical neutralization of aerosols. *Journal of Aerosol Science*, 5(5), 465–472.

Matsoukas, T., & Russell, M. (1997). Fokker-planck description of particle charging in ionized gases. *Physical Review E*, 55(1), 991.

Mayya, Y., Sapra, B., Khan, A., & Sunny, F. (2004). Aerosol removal by unipolar ionization in indoor environments. *Journal of Aerosol Science*, 35(8), 923–941.

McMurry, P., & Rader, D. (1985). Aerosol wall losses in electrically charged chambers. *Aerosol Science and Technology*, 4(3), 249–268.

Mick, H., Hospital, A., & Roth, P. (1991). Computer simulation of soot particle coagulation in low pressure flames. *Journal of Aerosol Science*, 22(7), 831–841.

Nakaso, K., Han, B., Ahn, K., Choi, M., & Okuyama, K. (2003). Synthesis of non-agglomerated nanoparticles by an electrospray assisted chemical vapor deposition (es-cvd) method. *Journal of Aerosol Science*, 34(7), 869–881.

Oron, A., & Seinfeld, J. H. (1989). The dynamic behavior of charged aerosols: Iii. simultaneous charging and coagulation. *Journal of Colloid and Interface Science*, 133(1), 80–90.

Palsmeier, J. F., & Loyalka, S. K. (2013). Evolution of charged aerosols: role of charge on coagulation. *Nuclear Technology*, 184(1), 78–95.

Park, S., Lee, K., Shimada, M., & Okuyama, K. (2005). Coagulation of bipolarly charged ultrafine aerosol particles. *Journal of Aerosol Science*, 36(7), 830–845.

Sapra, B., Mayya, Y., Khan, A., Sunny, F., Ganju, S., & Kushwaha, H. (2008). Aerosol studies in a nuclear aerosol test facility under different turbulence conditions. *Nuclear Technology*, 163(2), 228–244.

Shimada, M., Okuyama, K., Kousaka, Y., Okuyama, Y., & Seinfeld, J. H. (1989). Enhancement of brownian and turbulent diffusive deposition of charged aerosol particles in the presence of an electric field. *Journal of Colloid and Interface Science*, 128(1), 157–168.

Shimada, M., Okuyama, K., & Kousaka, Y. (1989). Influence of particle inertia on aerosol deposition in a stirred turbulent flow field. *Journal of Aerosol Science*, 20(4), 419–429.

Simones, M. P., & Loyalka, S. K. (2015). Measurements of charged aerosol coagulation. *Nuclear Technology*, 189(1), 45–62.

Simones, M. P., Loyalka, S. K., Duffy, C., MacLoughlin, R., Tatham, A., & Power, P. (2014). Measurement of the size and charge distribution of sodium chloride particles generated by an aeroneb pro® pharmaceutical nebulizer. *European Journal of Nanomedicine*, 6(1), 29–36.

Smith, M., Lee, K., & Matsoukas, T. (1999). Coagulation of charged aerosols. *Journal of Nanoparticle Research*, 1(2), 185–195.
Tinsley, B. (2008). The global atmospheric electric circuit and its effects on cloud microphysics. *Reports on Progress in Physics*, 71(6), 066801.
Tsai, C.-J., Lin, J.-S., Deshpande, C., & Liu, L.-C. (2005). Electrostatic charge measurement and charge neutralization of fine aerosol particles during the generation process. *Particle Particle Systems Characterization*, 22(5), 293–298.
Vemury, S., Janzen, C., & Pratsinis, S. E. (1997). Coagulation of symmetric and asymmetric bipolar aerosols. *Journal of Aerosol Science*, 28(4), 599–611.
Whitby, E. R., & McMurry, P. H. (1997). Modal aerosol dynamics modeling. *Aerosol Science and Technology*, 27(6), 673–688.
Williams, M.M.R., & Loyalka, S.K. Aerosol science: Theory and practice
Xiong, Y., Pratsinis, S. E., & Mastrangelo, S. V. (1992). The effect of ionic additives on aerosol coagulation. *Journal of colloid and interface science*, 153(1), 106–117.
Yu, F., & Turco, R. P. (1998). The formation and evolution of aerosols in stratospheric aircraft plumes: numerical simulations and comparisons with observations. *Journal of Geophysical Research: Atmospheres (1984-2012) 103 (D20)*, 25915–25934.
Zebel, G. (1958). Zur theorie der koagulation elektrisch ungeladener aerosole. *Kolloid-Zeitschrift*, 156(2), 102–107.